Applied Catalysis B: Environmental 342 (2024) 123381

Contents lists available at ScienceDirect

Applied Catalysis B: Environmental

journal homepage: www.elsevier.com/locate/apcatb

Construction of Z-scheme photocatalyst with p-n heterojunction of molecular semiconductors for enhanced photocatalytic water oxidation

Junqiang Li [a,b,c,d], Shoufeng Wang [a,b,c,d], Renfu Li [a], Bo Zhang [a,b,c,d], Xiao Xu [a,b,c], Zhuoyue Wang [a,b,c,d], Longtian Kang [a,b,c,*]

[a] Key Laboratory of Design and Assembly of Functional Nanostructures, and Fujian Provincial Key Laboratory of Nanomaterials, Fujian Institute of Research on the Structure of Matter, Chinese Academy of Sciences, Fuzhou, Fujian 350002, PR China
[b] Fujian Science & Technology Innovation Laboratory for Optoelectronic Information of China, Fuzhou, Fujian 350108, PR China
[c] University Chinese Academy of Science, Fujian College, Fuzhou 350002, PR China
[d] College of Chemistry, Fuzhou University, Fuzhou 350116, PR China

ARTICLE INFO

Keywords:
Perylene-3,4,9,10-tetracarboxylic dianhydride
Cobalt phthalocyanine
Molecular semiconductor
P/N type heterojunction
Z-Scheme heterojunction
Photocatalytic water oxidation

ABSTRACT

Here, the donor-acceptor organic composites of n-type perylene-3,4,9,10-tetracarboxylic dianhydride (PTCDA) and p-type cobalt phthalocyanine (CoPc) semiconductors are firstly synthesized and optimized for photocatalytic oxygen evolution (POE) as catalyst. The POE rate of 12.30 mmol·g^{-1}·h^{-1} with the apparent quantum yield of 4.00 % at 475 nm can be achieved under visible light (> 420 nm), as compared with 1.58 mmol.g^{-1}.h^{-1} of PTCDA. Under the full UV-Vis light (> 320 nm), the rate is up to 17.65 mmol·g^{-1}·h^{-1}. The systematical experiments clearly reveal the generation of dual-channel energy transfer of fluorescence resonance from CoPc to PTCDA and electron transfer from oxygen groups in PTCDA to Co atom in CoPc under UV-Vis light irradiation. Consequently, the formation of Z-scheme p/n heterojunction in CoPc/PTCDA composite greatly enhances the POE performance due to the lifetime increase of metal-ligand charge transfer exciton in CoPc (44.83 vs. 2.95 ps) and perylene cationic exciton (20.13 vs. 2.13 ps).

1. Introduction

In recent years, the solar energy-driving water splitting and/or CO_2 reduction has been considered as a promising approach to achieve the carbon neutrality [1–4]. As usual, these reactions involve in the two half-reactions of water reduction and oxidation in the aqueous phase. Among them, the photocatalytic oxygen evolution (POE) reaction, which occurs at a relatively high potential (> 1.23 eV) and overpotential, is usually a key step because of the sluggish four-electron transfer process, and seriously affects the activity and stability of photocatalytic system [5]. So far, a variety of semiconductors with a suitable energy level have been proposed to explore their POE performance. Among most of typical POE photocatalysts, e.g. TiO_2, $BiVO_4$, and WO_3, g-C_3N_4, their POE activity are usually suffered from the limit absorption visible-light, and have to be modified, doped or engineered [6–10]. Hence, the organic conjugated semiconductors with intrinsic visible light absorption, e.g. metal porphyrin, perylene (Pe) derivatives and corresponding MOF or COF polymers, have been intrigued increasing researchers [11–14]. In comparison, the performance of current photocatalysts is more hindered by the rapid annihilation of photogenerated electron/hole pairs. At present, many strategies have been explored to promote the efficient separation and transportation of photoinduced carries through defect control, metal or salt doping, the enhancement of crystal quality or build-in electric field (BIE), and heterojunction construction [14–19].

Among the aforementioned strategies, it has been enough confirmed that constructing heterojunction, especially direct Z-scheme p/n type heterostructures, is one of the most efficient routes for the spatial separation of photoinduced electron/hole pairs [20,21]. The first reason is the photoinduced electrons and holes can easily transfer in the n- and p-type semiconductors, respectively. The second one is that they can be quickly separated due to the existence of built-in electric field [22]. The third one is the strongest redox ability of heterojunction components can be kept to avoid the energy lost [23]. In addition, the corresponding composites usually possess wider absorption and higher stability than individual component. Therefore, the composites with Z-scheme p/n type heterojunction are actually a kind of perfect photocatalysts, and can exhibit more excellent photocatalytic activity than its component.

* Correspondence to: Fujian Institute of Research on the Structure of Matter, Chinese Academy of Sciences, Fuzhou, Fujian 350002, PR China.
E-mail address: longtiank@fjirsm.ac.cn (L. Kang).

https://doi.org/10.1016/j.apcatb.2023.123381
Received 30 August 2023; Received in revised form 23 September 2023; Accepted 8 October 2023
Available online 10 October 2023

For example, Zhang group reported the synthesis of Z-scheme Cu_3P/g-C_3N_4 composite with p-n chemical bond, and achieved the photocatalytic hydrogen evolution of 8.78 mmol·g^{-1}·h^{-1}, even 20.22 mmol·g^{-1}·h^{-1} with 0.5 wt% Pt [24]. Liu group prepared the Z-scheme $CsPbBr_3$ QD/$CuCo_2O_4$ NS p/n heterojunction and achieved 3.2 times and 9.2 times higher photocatalytic CO_2 to CH_4 than $CsPbBr_3$ QD and $CuCo_2O_4$ NS, respectively [25]. Bai group synthesized the Z-scheme Mn_3O_4/ Co_9S_8 with p/n type heterostructure, and obtained 1.6 mM of H_2O_2 for 6 h in alkaline medium without using electron donors and pure O_2 [26]. Our group synthesized the CoTPP/NGQDs Z-scheme heterojunction and firstly achieved the POE on the molecules in the aqueous colloid system [27]. Up to now, most works actually focus on the construction of polymer or inorganic Z-scheme p/n type heterojunctions for the photocatalytic reduction of water or CO_2, a few of pure molecule-based ones are prepared and applied in the photocatalytic water oxidation.[28–30] Besides the electron transfer between two components in heterojunction, the fluorescence resonance energy transfer (FRET), which occurs through the Coulomb interaction between donor and acceptor dipoles, is also one of the important ways of energy transfer [31]. For the heterojunction photocatalyst combining two kinds of conjugated chromophores, in theory, FRET process can efficiently enhance the photocatalytic activity of acceptor [32,33]. Therefore, the study on the synergic effect and mechanism of electron transfer and FRET in Z-scheme heterojunctions on photocatalytic activity should be of great significance. Unfortunately, the modes of dual-channel energy transfer during POE was investigated a few.

The perylene-based PTCDA molecule, as a classical planer conjugated n-type organic semiconductor, has attracted considerable attention on its potential and promising application in electronic and optoelectronic devices [34]. Its growth, interfacial electronic structure and/or interaction on different substrates, e.g. noble metal, graphene, TiO_2, Si, phthalocyanine (Pc), been widely studied [35]. However, the intrinsic low BIE and/or big size seriously restrict its optical and photoelectric properties [19,36]. A series of strategies, including the enhancement of crystallinity, coordination with metal ions, addition of metal salts or metal oxides, and/or introduction of functional groups, have been proved efficient to improve the POE activity of PTCDA and its derivatives as catalyst [19,37–39]. For example, the introduction of CoO_x clusters or $Co(NO_3)_2$ into 1D perylene diimide (PDI) polymers can markedly improve the lifetime and transportation of photoinduced carriers due to the heterojunction formation under the interaction between Co and N atoms [18,40]. The high-crystallinity PDI crystal with strong BIE can efficiently enhance dipole moment of the macromolecule, resulting in a 774.5-fold increase in photocatalytic activity [19]. With the suitable energy level and a strong visible absorption, the construction of donor/acceptor heterojunctions between PTCDA and other molecule semiconductors is thought as an efficient strategy for its application in organic light emitting diodes [41], organic photovoltaic cells [42], photocatalysis [4,14] etc. It has been proved that the formation of certain PTCDA/Pc heterojunction, e.g. PTCDA/ZnPc and PTCDA/CuPc, shows a marked tendency to the exciton dissociation due to the existence of high dipolar field [42,43]. Although the versatile chemicophysical properties and excellent performance of organic donor/acceptor composites have been widely investigated [44], to our best knowledge, the POE performance and mechanism of related composites was rarely reported under UV-Vis light irradiation.

In this work, the conjugated n-type PTCDA and p-type CoPc semiconductor molecules were directly applied as catalyst for POE with the complementary light absorption from UV, visible to the near-infrared range. The CoPc/PTCDA composites were synthesized and characterized, in which the preferential 1D nanostructures of CoPc and PTCDA alternately arise and disappear with the ratio decrease of CoPc to PTCDA. The heterojunction formation was carefully studied, confirming the interaction existence between CoPc and PTCDA. The effect of CoPc/PTCDA ratio on the optical, photoelectrical and electrical properties was systematically investigated. As compared the PTCDA nanorods (1.58 mmol·g^{-1}·h^{-1}), the optimal CoPc/PTCDA sample as catalyst exhibited the POE rate of 12.30 and 17.65 mmol·g^{-1}·h^{-1} under the visible light irradiation ($\lambda > 420$ nm) and UV–vis light ($\lambda > 320$ nm), respectively. The energy level structures of CoPc and PTCDA and the femtosecond transient absorption (fsTA) spectra clearly revealed the existence of dual-channel energy transfer of FRET and electron transfer between CoPc and PTCDA after the formation of Z-scheme p/n type heterojunction. This work provides a promising strategy to construct molecular-based heterojunction as the outstanding photocatalysts.

2. Experimental section

2.1. Materials

3,4,9,10-perylenetetracarboxylic dianhydride (PTCDA, 98.0 %) and cobalt(II) phthalocyanine (CoPc, 95.0 %) were obtained from J&K Chemicals Co. Ferric nitrate nonahydrate ($Fe(NO_3)_3$·9 H_2O, 98.5 %), silver nitrate ($AgNO_3$, 99.8 %) and concentrated sulfuric acid (H_2SO_4, 98.0 %) were purchased from Sinopharm Chemical Reagent Co., Ltd. (Shanghai, China). The ultrapure water was produced with a Water Purifier apparatus (WP-UP-IV-20).

2.2. Synthesis of CoPc, PTCDA and CoPc/PTCDA composites

In a typical test, CoPc (57.1 mg, 0.1 mmol) and PTCDA (39.2 mg, 0.1 mmol) were dispersed in 98 % concentrated H_2SO_4 (100 mL). Then 1.0 mL of CoPc+PTCDA mixed solution was injected into 5.0 mL deionized water with an ice-water bath and ultrasonication, and aged for 12 h. The 1:1 CoPc/PTCDA composite can be obtained through the centrifugation at 10,000 rpm for 10 min, and then was washed four times with deionized water, finally dried at 80 °C. The CoPc and PTCDA nanomaterials and different CoPc/PTCDA composites with mole ratio of 1:0, 8:1, 4:1, 1:2, 1:4, 1:6, 1:8 and 0:1 can be prepared through adjusting the mole ratio of CoPc to PTCDA, when the total mole concentration was kept at 1.0 mM in concentrated H_2SO_4.

2.3. Measurement of photocatalytic activity

Typically, 3.0 mg CoPc/PTCDA sample as photocatalyst was dispersed in 100 mL water, including 5.0 mM $AgNO_3$ as sacrificial agents, to form a colloid system with stirring. Then, it was transferred into the reaction vessel. The glass reactor was connected to the photocatalytic system (Perfect Light, Labsolar-6A) and degassed under vacuum conditions for 20 min. The POE test was carried out under the irradiation of a 300 W Xe lamp (Perfect Light, PLS-SXE300BF) without/with a 420 nm cut-off filter. The evolved oxygen was detected with an on-line gas chromatograph (Techcomp, GC7900). After the photocatalytic activity was measured at the wavelength of 420, 450, 475, 500, 550, 600, and 700 nm with 10 mg catalyst, the AQY was calculated according to the following formula, respectively.

$$\mathrm{AQY}(\%) = \frac{4 \times \text{number evolved of} O_2 \text{molecules}}{\text{number of incident photons}} = \frac{4 \times n \times N_A}{S \times P \times t \times \frac{\lambda}{h \times c}} = \frac{4 \times n \times N_A \times h \times c}{S \times P \times t \times \lambda}$$

In the equation, n represents the molar amount of O_2 generated during the photocatalytic process (μmol), N_A stands for Avogadro's constant (6.02×10^{23} /mol), S denotes the area of light irradiation (26.4 cm^2), P signifies the light intensity parameter obtained from the light power measurement (mW·cm^{-2}), t stands for the reaction time under visible light irradiation (in seconds), λ means the wavelength (nm), h represents the value of Planck's constant as 6.626×10^{-34} J·s, and c denotes the speed of light as 3×10^8 m/s.

2.4. Photoelectrochemical and electrochemical measurement

The customary and standardized three-electrode was employed for the electrochemical test in a 0.5 M Na_2SO_4 solution, containing a counter electrode (carbon rod), a reference electrode (Ag/AgCl electrode), and a working electrode. The working electrode was prepared through the following steps. Firstly, 5.0 mg sample was dispersed into 1.0 mL of a Nafion/H_2O solution (V_{Nafion}: V_{H2O}=1:9) and formed the homogeneous suspension. Subsequently, the suspension was carefully coated onto ITO conductive glass (1.5 cm * 1.5 cm), and dried at 50 °C for 12 h. Finally, the three electrodes were assembled with a CHI760E electrochemical workstation (Chenhua Instruments, Shanghai, China). During the photocurrent test, a 300 W Xe lamp ($\lambda > 420$ nm) was employed as the light source. For the electrochemical impedance test, 100 μL of CoPc/PTCDA suspension was coated onto both sides of hydrophilic carbon paper (1.0 cm * 1.0 cm) as the working electrode.

3. Result and discussion

3.1. Morphology, structure and component characterization

The preparation of CoPc, PTCDA and CoPc/PTCDA nanostructures were carried out through two steps of protonation in concentrated H_2SO_4 (98 %) of CoPc and PTCDA and hydrolysis [45]. In a typical experiment, 1.0 mL of 1.0 mM CoPc+PTCDA/H_2SO_4 mixed solution was quickly injected into 5.0 mL deionized water with stirring. The mole ratio of CoPc to PTCDA was adjusted to obtain the different CoPc/PTCDA composites. The detailed process can be found in the Experimental Section. The typical SEM images of CoPc and PTCDA nanomaterials and as-obtained CoPc/PTCDA composites are shown in Fig. 1 and Figs. S1-S8. The Fig. S1 and Fig. S2 suggests that the CoPc and PTCDA conjugated molecules intent to self-assemble into one-dimensional (1D) structure due to the strong intermolecular π-π interaction (see Fig. 1a-b). When the mole ratio of CoPc to PTCDA is 8:1, the regular and clear nanowires with the average diameter of ~ 50 nm can be prepared, as displayed in Fig. S3. With the ratio of CoPc/PTCDA is decreased to 4:1, a large amount of rough short nanorods and a few amounts of nanoparticles can be found (see Fig. 1c and Fig. S4). When the CoPc/PTCDA is 1:1, Fig. 1d and Fig. S5 present 1D nanostructures with the average diameter of ~ 100 nm form, accompanied with the generation of more nanoparticles. Fig. 1e and Fig. S6 shows that a lot of ~50 nm nanoparticles and 1D structure with the average diameter of ~1.0 μm generate in the CoPc/PTCDA composite with the ratio decrease of CoPc/PTCDA to 1:2. The diameter of 1D structure reduces to ~300 nm when the mole ratio of CoPc/PTCDA is 1:4. With the ratio is decreased from 1:6–1:8, the diameter changes from ~200 nm to < 50 nm. In addition, the nanoparticles seemly disappear in Fig. 1g, Fig. 1h, Fig. S7, and Fig. S8.

The size, structure and component of CoPc/PDA composite can be detected through TEM and corresponding element mappings. In Fig. 2, the diameters of nanorods in 4:1 and 1:8 CoPc/PTCDA composites are ~50 nm and ~30 nm, which are consistent with those in their SEM images. Here, no obvious nanoparticles can be observed in the two samples. The inset high-resolution TEM images in Fig. 2a and Fig. 2c reveal that these nanorods have high crystallinity. The d-spacing of 1.25 nm in Fig. 2a may be assigned to the (100) facet of CoPc single

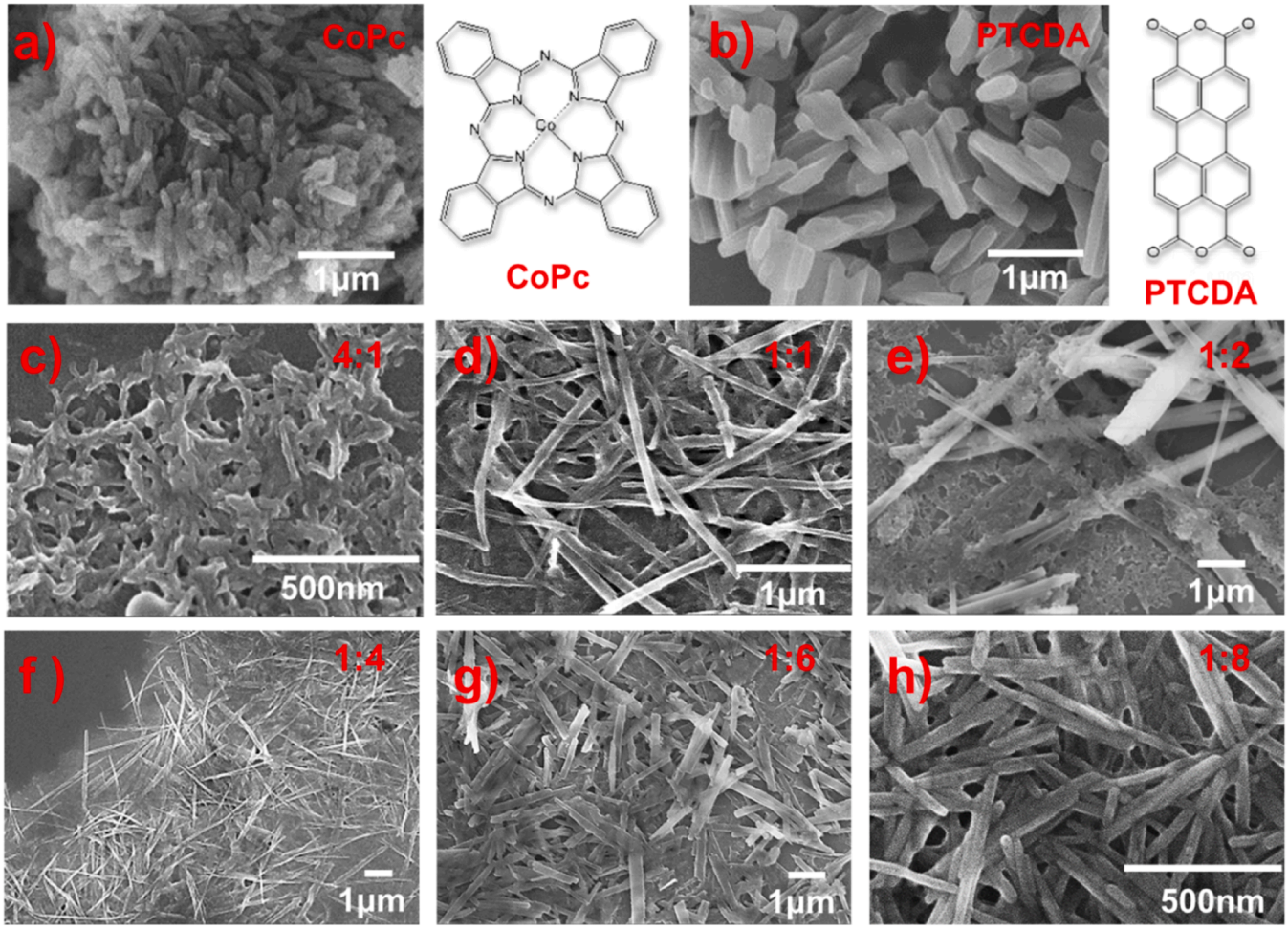

Fig. 1. SEM images of a) CoPc nanorods, b) PTCDA nanorods, and CoPc/PTCDA composites with different ratios of c) 4:1, d) 1:1, e) 1:2, f) 1:4, g) 1:6, h) 1:8.

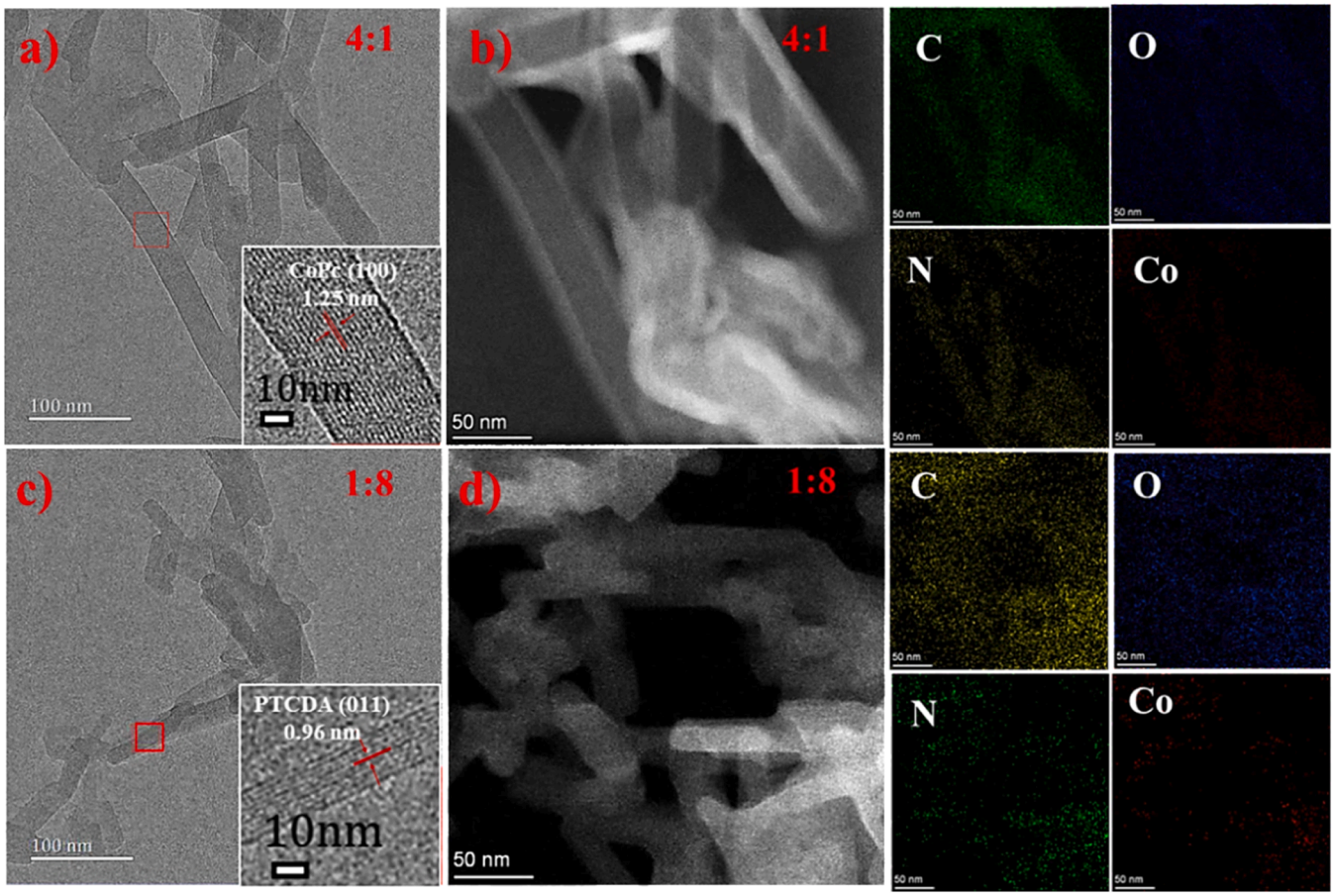

Fig. 2. TEM images and element mappings of 4:1 (a-b) and 1:8 (c-d) CoPc/PTCDA composites.

crystal, while the d-spacing of 0.97 nm Fig. 2c may be indexed to the (011) facet of PTCDA crystal. In theory, the Co and N atom only exists in CoPc, and the O atom is from PTCDA and/or residual H_2SO_4, as shown in Fig. 1. The co-existence of C, O, N and Co elements in the as-obtained nanorods confirms the successful recombination of CoPc and PTCDA, suggesting the existence of strong interaction between CoPc and PTCDA. The difference in element mappings is that the outline of nanorods 4:1CoPc/PTCDA sample is clearer than that in 1:8 CoPc/PTCDA sample owing to more CoPc containing heave metal Co. Combining the above SEM, TEM, and element analysis in Fig. 1 and Fig. 2, it can be proved that the 1D nanostructure and nanoparticles should be PTCDA and CoPc in 4:1 CoPc/PTCDA composite, and should be CoPc and PTCDA in 1:8 CoPc/PTCDA composite, respectively. With the decrease of CoPc/PTCDA ratio, the above evolution process of CoPc/PTCDA structure strongly indicates the formation and disappearance of CoPc 1D nanostructures and PTCDA nanoparticles, the subsequent generation of CoPc nanoparticles and PTCDA 1D nanostructures.

To further understand the change of structure and component in the CoPc/PTCDA composites, the X-ray diffraction (XRD) of different samples were measured, as seen in Fig. 3 and Fig. S9. The peaks at 6.97°, 7.21°, 15.81°, 24.03°, 26.79°, and 27.65° correspond to the (001), (100), (102), (1 $\bar{}$10), (21 $\bar{}$0), and (21 $\bar{}$1) crystal facets of α-CoPc (PDF #44-1994) [46,47]. The peaks at 12.29°, 24.63°, and 27.59° belong to the (021), (042), and (10 $\bar{}$3) crystal facets of PTCDA (CCDC No. SUWMIG02) [48]. With the ratio of CoPc/PTCDA decreased from 4:1 to 1:4, the gradual disappearance of typical XRD peaks of CoPc crystal at 6.97° and 7.21° and the slow generation of typical XRD peak of PTCDA at 12.29° directly confirm the evolution process of PTCDA and CoPc amorphous nanoparticles and their 1D nanocrystals [40,49]. When the ratio is less than 1:4, the XRD peaks of CoPc (001) and (100) facets become weaker and gradually disappear, while the XRD peaks of PTCDA crystal enhance. These phenomena strongly suggest that most of CoPc aggregates should disappear, and CoPc molecules should adsorb on the surface of PTCDA crystal in 1:4 CoPc/PTCDA composite. Besides, it can be observed that the XRD peak of PTCDA (10 $\bar{}$3) facet shifts from 27.59° to 27.19° when the CoPc/PTCDA ratio is 1:6 and 1:8. For PTCDA single crystal, the d-spacing increase of (10 $\bar{}$3) facet corresponds to the loosing of π-π stacking of perylene moiety, as shown in Fig. S9. Basing on the size change of PTCDA in 1:6 and 1:8 CoPc/PTCDA samples in Fig. 1 and their conjugated molecular structures, one reasons may result from the size effect, the other reason may derive from the formation of CoPc/PTCDA co-crystal structure [50]. As a result, the photocatalytic performance may degrade due to the reduction of intermolecular charge transfer and the separation efficiency of photoinduced electrons and holes [19]. The above experimental results are well agreeing with the evolution process of CoPc/PTCDA composites in Fig. 1 and element distribution in Fig. 2. In general, the CoPc/PTCDA heterojuction can form well when the ratio of CoPc/PTCDA is more than 4:1 or less than 1:4, that is before the formation of individual CoPc or PTCDA aggregates due to intermolecular interaction [44].

To investigate the interaction between CoPc and PTCDA molecules in the CoPc/PTCDA composites, their component and chemical states in the typical CoPc/PTCDA composites were studied through Fourier transform infrared spectroscopy (FT-IR) and X-ray photoelectron spectroscopy (XPS). In the FT-IR spectrum of PTCDA in Fig. 3b, two strong characteristic peaks of PTCDA at 1756 cm^{-1} and 1730 cm^{-1} correspond to the symmetric and asymmetric stretching vibrations of C═O bond [40]. The peaks at 1593, 1506, and 1406 cm^{-1} can be assigned to the breathing vibration of aromatic ring connected with C═O group [40]. The stretching vibration of C-O bond can be seen at 1300 and 1234 cm^{-1}

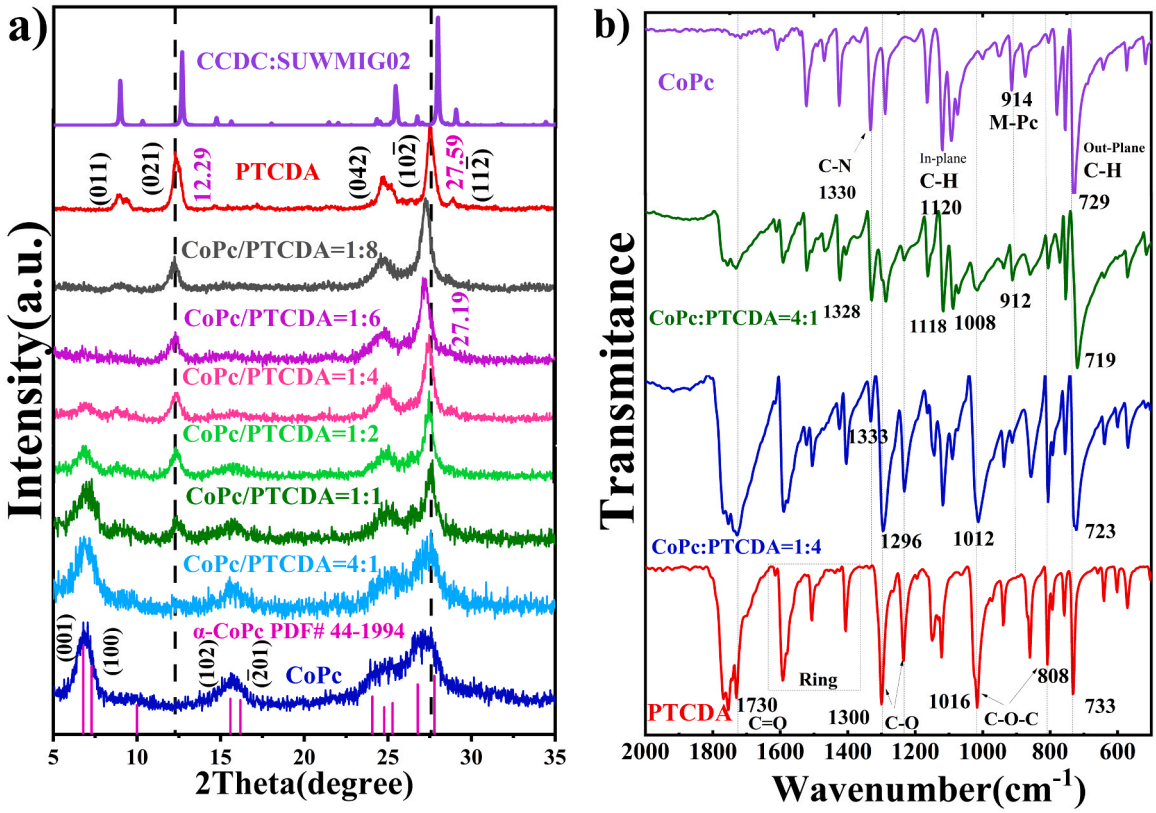

Fig. 3. a) XRD patterns and b) FT-IR spectra of PTCDA, CoPc, and CoPc/PTCDA composites.

[51,52]. The peaks at 1016 and 808 cm^{-1} are from the stretching vibration of acid anhydride (O═C-O-C═O) [51,52]. In the FT-IR spectrum of CoPc, the peak at 1330 cm^{-1} can be attributed to the stretching vibration of C–N bond [53]. The peaks at 1120 and 729 result from the in-plane and out plane bending vibration of C-H bond, respectively. The typical peak of metal-Pc can be observed at 914 cm^{-1} [54]. In the CoPc/PTCDA composites, the corresponding peaks of CoPc and PTCDA can be found and their intensity depends on the ratio of CoPc to PTCDA. As compared the FT-IR spectra of individual CoPc and PTCDA, there are three obvious changes. 1) The asymmetric stretching vibrations of C═O bond at 1730 cm^{-1} enhances, and is stronger than its symmetric stretching vibrations at 1750 cm^{-1}. 2) The out-plane bending vibration of C-H bond between 710 and 740 cm^{-1} becomes weak. 3) The C-O-C vibration reduce from 1016 cm^{-1} in PTCDA to 1012 cm^{-1} in 1:4 CoPc/PTCDA composite, to 1008 cm^{-1} in 4:1 CoPc/PTCDA composite. The above phenomena indicate the existence of hydrogen bond besides π-π interaction between CoPc and PTCDA molecules [55]. As a result, the CoPc and PTCDA form the heterojunction in the 4:1, 1:4, 1:6 and 1:8 CoPc/PTCDA composites.

The full XPS spectrum of CoPc/PTCDA composite in Fig. S10 shows the binding energy of Co, N, C and O atoms, indicating the existence and successful recombination of CoPc and PTCDA. In Fig. 4a, the high-resolution C 1 s spectra of PTCDA can be divided into the aromatic ring (C-C/C═C, 284.80 eV), edge C (C-(C═O), 285.60 eV), and carbonyl group (C═O, 289.32 eV) [19]. The C1s spectrum of CoPc can be divided into three peaks from the C-C bond in benzene rings at 284.8 eV, the C-N bond at 285.90 eV and the C═N bond at 287.4 eV [56]. The binding energy of different C1s components does not obviously change in CoPc/PTCDA composites, meaning that the carbon skeletons of CoPc and PTCDA are stable. The N1s XPS spectra of CoPc in Fig. 4c have the two peaks of pyridine N (399.07 eV) and pyrrole N (C-N-Co, 399.81 eV) [56]. The binding energy of pyrrole N decreases to 399.56 eV in the CoPc/PTCDA composite, meaning the electron transfer from Co to N atom. Two peaks of Co 2p at 780.60 and 795.99 eV in Fig. 3d together with their satellite peaks derive from the electron transition of $2p_{1/2}$ and $2p_{3/2}$ orbits of Co^{2+} [57]. The increase of Co 2p binding energy in CoPc/PTCDA indicates the increase of Co^{2+} rather than Co^{3+} [58]. Hence, the central Co atom in CoPc should accept electron, too. The high-resolution O 1 s XPS peaks of PTCDA in Fig. 4b can be separated into three peaks of C═O group at 531.22 eV, C-O-C group at 532.41 eV, and water at 534.06 eV. It can be found that the O 1 s binding energy of C═O and C-O-C groups in CoPc/PTCDA increases by 0.45 and 0.30 eV, respectively. Because the C1s binding energy does not obviously change, the above change of binding energy of N 1 s, Co 2p and O 1 s strongly indicates that the electron transfer should occur from O atom to Co atom, then to N atom. Combining the FT-IR and XPS results, it can be speculated that the interaction between CoPc and PTCDA should derive from the electron transfer from O atom in PTCDA to Co and H atoms in CoPc besides π-π interaction. Therefore, the self-assembling of CoPc or PTCDA molecules into 1D structures should be not only limited due to the decrease of their monomer concentration in CoPc+PTCDA/H_2SO_4 solution, but also be suppressed by the strong interaction between CoPc and PTCDA molecules. These should be the key reasons why the CoPc/PTCDA heterojunction can generate.

3.2. *Optical, photoelectric and electrical properties*

To obtain the optimal optical, electrical and photoelectrical properties of CoPc/PTCDA composites, the UV-Vis absorption, photoluminescence (PL), photocurrent and electrochemical impedance spectroscopy (EIS) of different samples were measured and analyzed. In Fig. 5a. The UV-Vis absorption of PTCDA between 300 and 520 nm originates from the electron transition of n→π* and π→π*. Among them, the absorption peak at ~420, ~450, ~465 and ~500 nm can be attributed to the 0–3, 0–2, 0–1, 0–0 models stretching vibration coupled with the π→π * electronic transition of perylene moiety [40]. The peak

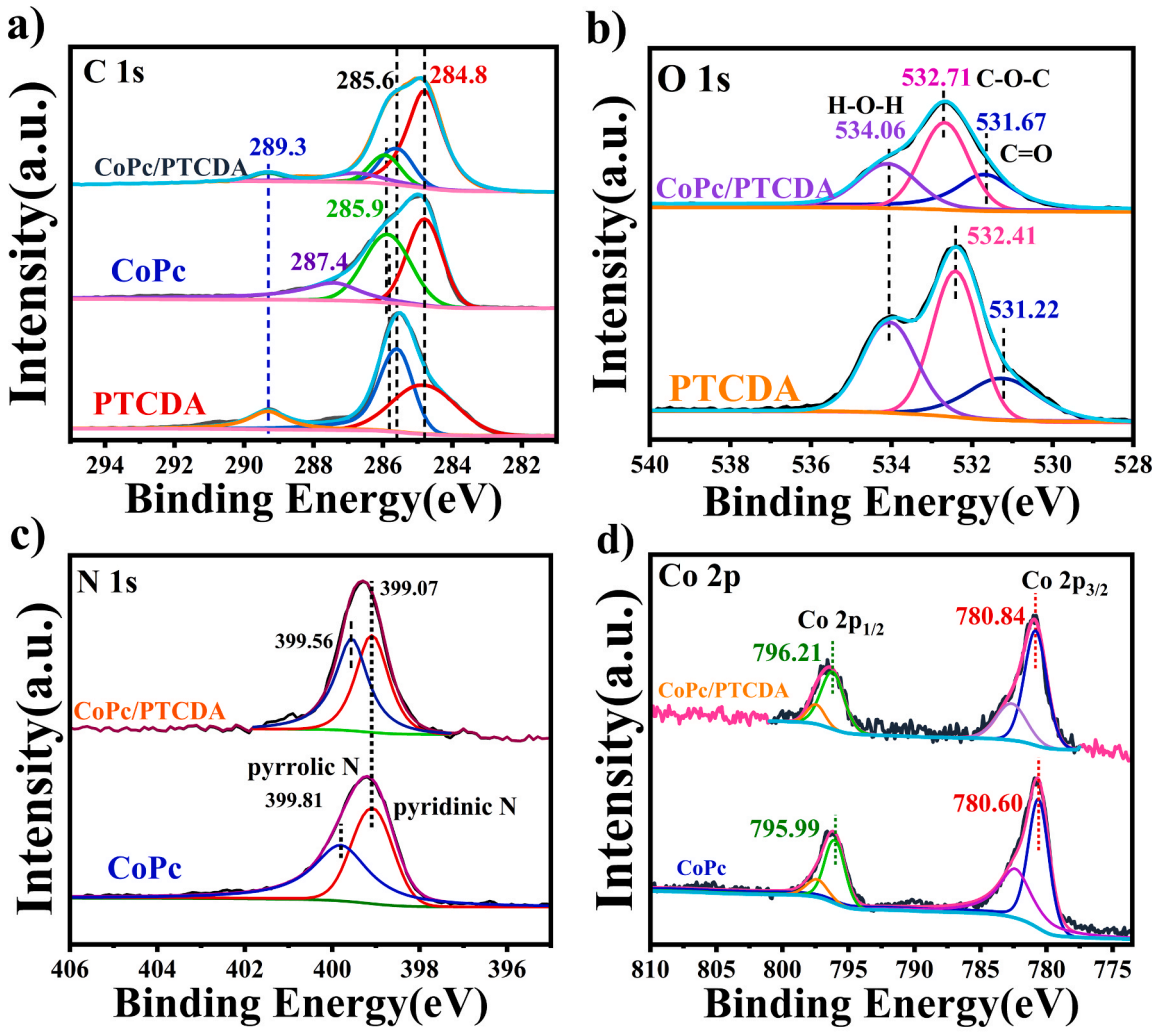

Fig. 4. High-resolution XPS spectra of a) C 1 s, b) O 1 s, c) N 1 s and d) Co 2p in CoPc, PTCDA and CoPc/PTCDA composite.

at 555 nm can be assigned to the intermolecular charge transfer state due to the formation of aggregate. The absorption peaks of CoPc at the range of 300–400 nm, 609 and 680 nm correspond to the Soret band and Q band absorption, respectively [59]. For the UV-Vis adsorption of CoPc/PTCDA composites, the characteristic peaks of both CoPc and PTCDA can be found in every sample. Besides, two obvious phenomena can be observed. One is that the intensity change is consistent with the component amount in CoPc/PTCDA composites. Another is that the width of main absorption peak at 400–530 nm (or 500–800 nm) becomes narrow with the decrease of component amount of PTCDA (or CoPc) in CoPc/PTCDA, meaning the gradual disappearance of corresponding aggregates. These changes are in keeping with their morphology and structure shown in Fig. 1 and Fig. 3, further confirming that CoPc and PTCDA have been successfully recombined with the ratio change of CoPc/PTCDA from 8:1 to 1:8. In addition, it can found that the CoPc/PTCDA composites have wide light absorption from 300 nm to 700 nm, and can be better matched to sunlight spectrum when the CoPc/PTCDA ratio is less than 1:2.

Fig. 5b and Fig. S11 exhibits the PL spectra of different samples upon the excitation light of 375 nm and 480 nm. The PL peaks at ~ 426 nm and ~699 nm derive from the de-excited emission of CoPc exciton, while the peaks at ~537 nm and ~578 nm are from PTCDA. An interesting phenomenon is that the corresponding intensity of PTCDA PL spectra is not coincided with its amount in CoPc/PTCDA composites like that of CoPc PL spectra. The 1:4 CoPc/PTCDA sample displays the weakest PL intensity. Meanwhile, the PL spectrum of CoPc is overlap with the absorption of PTCDA between 400 nm and 550 nm, strongly indicating the FRET from CoPc to PTCDA under the UV light of < 400 nm irradiation. It also means that after the formation of CoPc/PTCDA heterojunction, more PTCDA exciton (photoinduced electron/hole pairs) can generate under the irradiation of solar UV light through FRET process. This may be the main reason why the PL intensity of PTCDA in 1:1 and 1:2 CoPc/PTCDA composites is stronger than that in 1:4 CoPc/PTCDA composite. In theory, the FRET from CoPc to PTCDA is beneficial to the photocatalytic reaction on acceptor PTCDA [32]. The effect of CoPc/PTCDA heterojunction on the photoelectric conversion was investigated through the measurement of transient photocurrent response, as shown in Fig. 5c. The positive and negative values of transient photocurrent reveal that the major charge carriers are holes in CoPc and electrons in PTCDA on the basis of the properties of semiconductor. These results also suggest that CoPc and PTCDA are p-type and n-type semiconductors, respectively. For CoPc/PTCDA composites, all of photocurrent values are negative and stable, like that of PTCDA. It means that the major photoinduced carriers should be electrons from excited and enhanced PTCDA in the CoPc/PTCDA composite, and the electron transfer from PTCDA to CoPc should occur through the Co-O interaction, combining with the XPS results. The 1:4 CoPc/PTCDA composite exhibits the strongest photocurrent, indicating the best efficiency of separation and transportation of photoinduced carriers. In order to easily understand and further explore the formation of p/n type CoPc/PTCDA heterojunction, the Mott-Schottky plots of CoPc, PTCDA and CoPc/PTCDA composite are measured and analyzed, as shown in

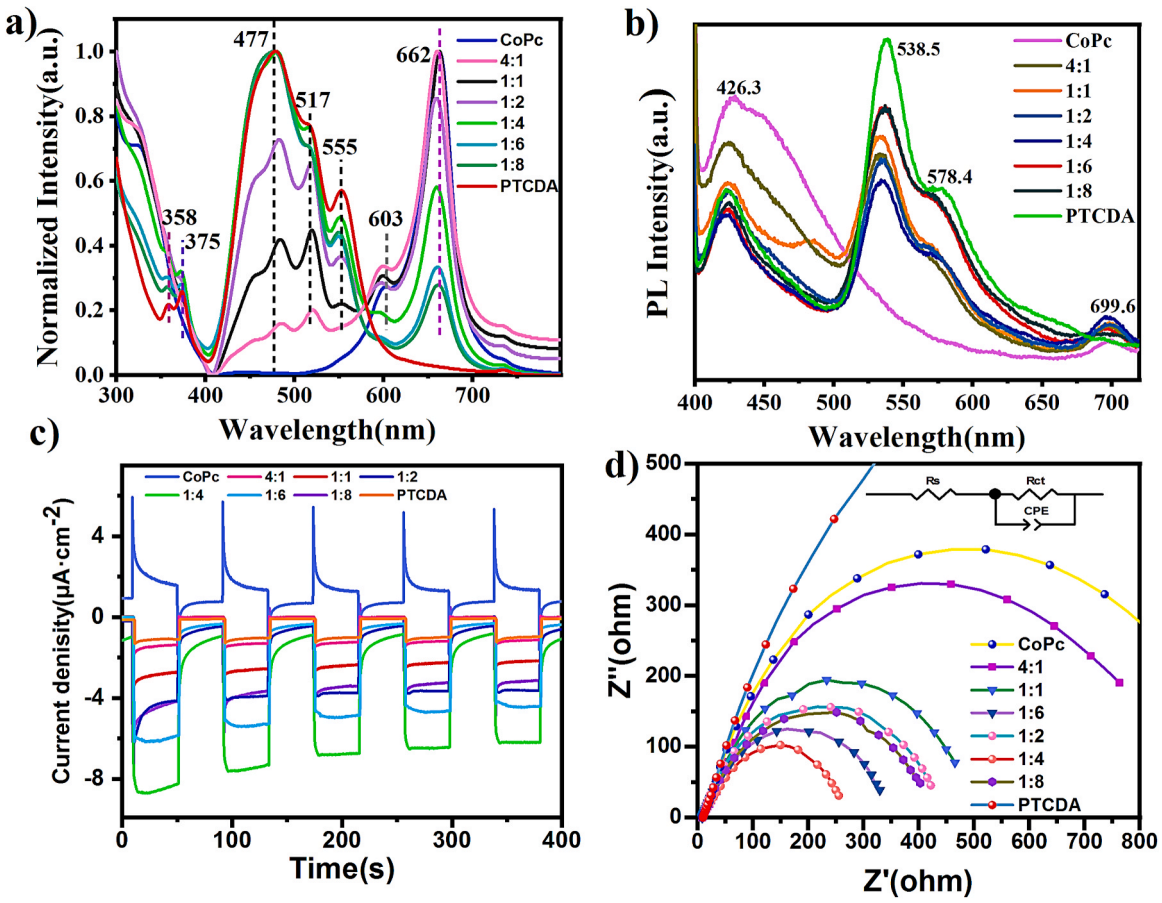

Fig. 5. a) UV–vis spectra of PTCDA, CoPc, and CoPc/PTCDA composites dispersed in DMSO. b) Photoluminescence(PL) spectra ($\lambda_{ex.}$= 375 nm). c) Transient photocurrent, and d) Electrochemical impedance spectroscopy.

Fig. S12. The negative slope of CoPc and the positive one of PTCDA clearly reveal that CoPc and PTCDA should be the p-type and n-type organic semiconductor, respectively [60,61]. For the CoPc/PTCDA composite, the Mott-Schottky plot exhibits a typical inverted "V-shape", meaning the formation of p/n heterojunction [61]. According to the Mott-Schottky equation, it can be found that there is the higher current density in PTCDA than CoPc because the absolute value of slope is bigger in Fig. S12. This may be the reason why the photocurrent of CoPc/PTCDA composites is negative. In Fig. 5d, the lowest EIS of 1:4 CoPc/PTCDA composite further proves that it has the best ability of electron transportation. Basing on the photocatalytic mechanism, the wider light absorption, stronger photocurrent, and lower PL intensity and EIS value of 1:4 CoPc/PTCDA composite than other samples imply that it should have more excellent photocatalytic performance.

3.3. Photocatalytic oxygen evolution

Owing to the excellent POE performance of perylene-based materials [28], we studied the photocatalytic activity of the CoPc/PTCDA p/n heterojunction. In a typical test, 5.0 mg sample was dispersed into 100 mL of water, including 5.0 mM of $AgNO_3$ as an electron acceptor. The 300 W Xe lamp was used as light source. The POE rate were recorded every 30 min. The detailed test can be seen in Experimental section. The POE rate was measured and shown in Fig. 6a-c. Here, the experiment was repeated three times, and the average value was demonstrated. It can be found that the change of oxygen evolution increases with time. The gradual decrease of POE rate with time can be attributed to the decrease of $AgNO_3$ and the generation of Ag particles on the surface of photocatalyst [40]. No sign of oxygen evolution can be detected when CoPc nanorods acts as photocatalyst. Under the visible light irradiation ($\lambda > 420$ nm), PTCDA nanorods as photocatalyst exhibits the POE rate of 1.58 mmol·g^{-1}·h^{-1}. With the CoPc/PTCDA composite as photocatalyst, Fig. 6a displays that the POE rate first increases, and then decreases when the CoPc/PTCDA ratio decreases from 4:1 to 1:8. The highest POE rate of 12.30 mmol·g^{-1}·h^{-1} can be achieved with 1:4 CoPc/PTCDA composite as photocatalyst, which is ~8 times more than that with pure PTCDA as catalyst. This trend is in accordance with the PL and transient photocurrent results. The above experimental results also suggest that PTCDA should be the active center, and CoPc should promote the POE performance of PTCDA. To investigate the effect of FRET from CoPc to PTCDA on the POE activity of PTCDA, the POE activity of 1:4 CoPc/PTCDA was tested under full-spectrum light ($\lambda > 320$ nm) irradiation, as seen in Fig. 6b. The POE rate increases by ~43 % to 17.56 mmol·g^{-1}·h^{-1}, which is ~9 times POE rate of pure PTCDA (1.98 mmol·g^{-1}·h^{-1}). It also indicates the positive effect of FRET from CoPc to PTCDA on POE activity of PTCDA besides the light absorption of PTCDA between 320 and 420 nm. To clearly identify the activity of different samples under light irradiation, the values of POE rate are summarized in Fig. 6c.

In order to study the influence of experimental conditions in the POE activity, different tests were carried out under no photocatalyst, no light, and/or no sacrificial agent (see Fig. S13) with 1:4 CoPc/PTCDA as photocatalyst. Obviously, no detectable oxygen can be obtained without light or electron sacrificial agent. Due to stronger ability of Ag^+ ion than Fe^{3+} to accept electron, only 5.82 mmol·g^{-1}·h^{-1}can be achieved with $Fe(NO_3)_3$ as the sacrificial agent. The system stability under visible light irradiation was evaluated through three cycle tests, as shown in Fig. 6d. After a test every two hours, the photocatalyst was centrifuged and collected, then washed with 1.0 mM HNO_3 to remove Ag particles. The as-obtained sample was used as photocatalyst again. The slight decrease

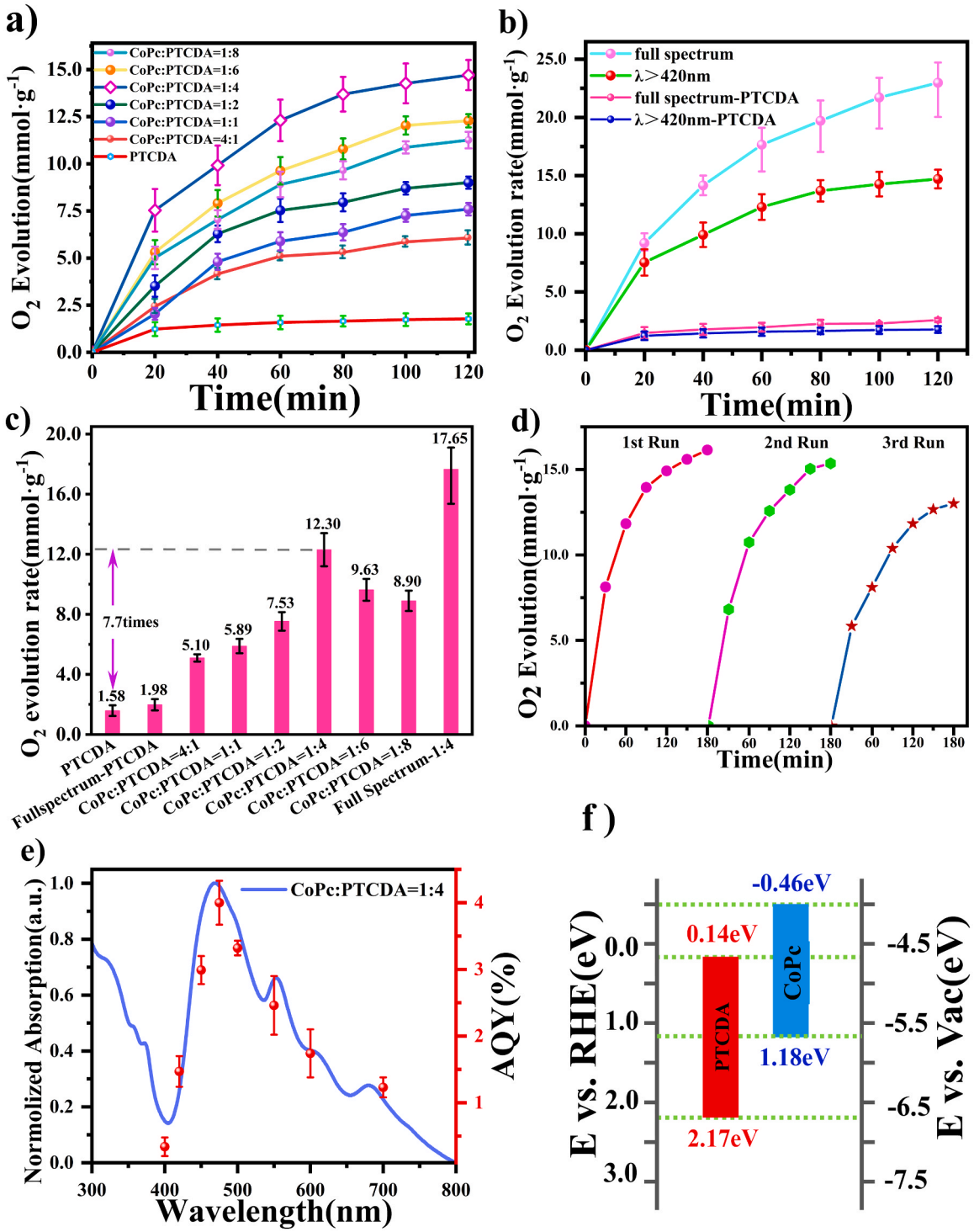

Fig. 6. a) Photocatalytic oxygen evolution of PTCDA and different CoPc/PTCDA composites, b) Photocatalytic POE rate of PTCDA and 1:4 CoPc/PTCDA composite under visible light (λ > 420 nm)and full spectrum (λ > 320 nm), c) POE activity under different test conditions, d) Cycling experiments with 1:4 CoPc/PTCDA composite as photocatalyst for 9 h, e) UV–visible spectrum of 1:4 CoPc/PTCDA composite dispersed in water and its AQYs at various wavelengths. Error bars were calculated as a percentage uncertainty on the basis of three repeated measurement, f) Energy band structure of CoPc and PTCDA.

of POE activity can be attributed to the loss of photocatalyst and the existence of residual Ag particles. In addition, the AQY at the wavelengths of 420, 450, 475, 500, 550, 600, and 700 nm were measured, respectively. Fig. 6e and Table S1 show that the AQY results are consistent with the light absorption of 1:4 CoPc/PTCDA composite in the aqueous phase. The highest AQY of 4.00 % can be obtained at 475 nm, which corresponds to the maximal light absorption of PTCDA as photocatalyst (see Fig. 3a).

To study the CoPc/PTCDA heterojunction and POE mechanism, the energy level of CoPc and PTCDA were measured through UV–visible diffuse reflectance spectrum (UV–vis DRS) and VB-XPS. Basing on the intercept of tangent to the Tauc plot of $(\alpha h\nu)^2$ vs. $h\nu$ in Fig. S14, the band gaps (E_g) of PTCDA and CoPc can be determined to be 2.03 eV and 1.64 eV, respectively [40]. The VB-XPS spectra reveal that the valence

band potentials (E_{VB}) of PTCDA and CoPc are 2.17 and 1.18 eV vs. RHE. Correspondingly, their conduction band potentials (E_{CB}) are 0.14 and − 0.46 eV vs. RHE according to the formula of $E_g = E_{VB}-E_{CB}$. Obviously, the oxygen product only generates on the surface of PTCDA due to the CoPc E_{HUMO} is lower than the lowest energy level of water oxidation (H_2O/O_2, 1.23 eV vs. RHE). It also means that the photoinduced electrons should transmit from PTCDA LUMO to CoPc HOMO through the Co-O bond and/or hydrogen bond during the POE process [62], and that the CoPc/PTCDA composite should be Z-scheme heterojunction. Subsequently, water is oxidized to O_2 by the photoinduced holes on PTCDA, while $AgNO_3$ is reduced to Ag by the photoinduced electrons on CoPc.

3.4. Photoelectric mechanism

To gain sight into the photoinduced electron transfer in CoPc/PTCDA heterojunction and further understand the POE mechanism, the fsTA spectra of CoPc, PTCDA and 1:4 CoPc/PTCDA composite were measured with pump laser light of 390 nm, as seen in Fig. 7a-c. Here, the fsTA kinetics of negative GB peak presents the lifetime of charge separation (τ_{CS}), while the kinetics of positive ESA peaks reflects the lifetime of charge recombination (τ_{CR}). The corresponding results can be found in Fig. 7d-f. In the fsTA spectra of CoPc (Fig. 7a), the peaks at 479 nm and 515 nm can be assigned to the excited-state absorption (ESA) because of the π electrons transmit in Pc ring from S_1 state to S_n state ($S_1 \rightarrow S_n$). The negative ground-state bleaching (GB) peaks at 560 nm and 609 nm generate due to the electron transfer from Pc ligand to Co atom (LMCT),

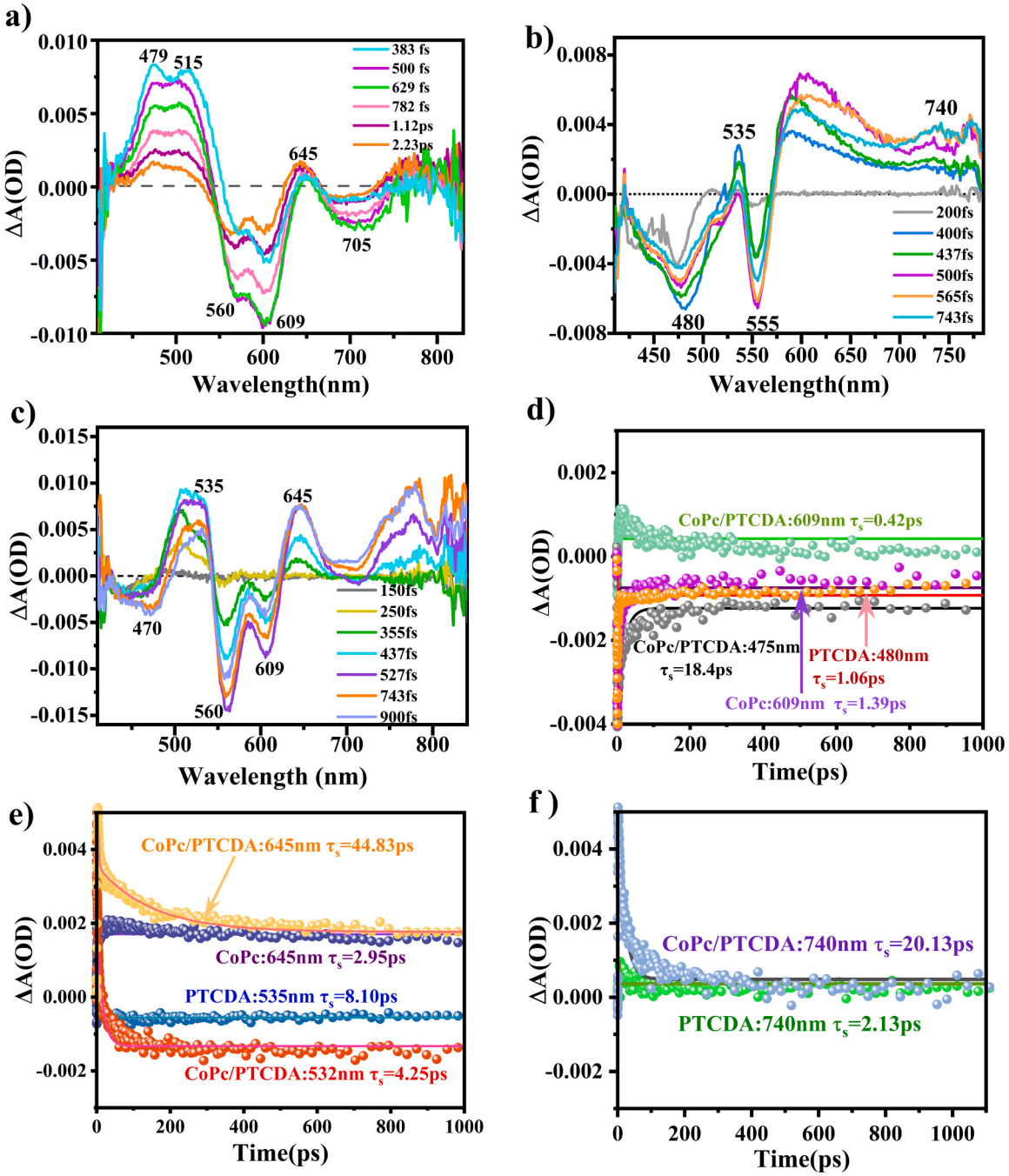

Fig. 7. The transient absorption spectra of a) CoPc, b) PTCDA, c) CoPc/PTCDA. d-f) fsTA kinetics lifetimes.

accompanied by the appearance of positive absorption peak of LMCT* state at 600–800 nm owing to the $T_1 \rightarrow T_n$ electron transition. Meanwhile, the appearance of negative stimulated emission (SE) peak at ~700 nm derives from the de-excitation emission of excitons, that is, the $S_1 \rightarrow S_0$ electron transition, as shown in Fig. 5b. The stronger ESA peak of Pc* than LMCT* also indicates that only a few amount of photoinduced electrons transfer from Pc to Co atom (Pc → Co). In the fsTA spectra of PTCDA (Fig. 7b), the negative GB peaks at ~480 nm and ~555 nm result from the light absorption of perylene ring and aggregate due to the electron transition of $S_0 \rightarrow S_1$ and the intermolecular charge transfer (IMCT). The generation of positive ESA peaks at ~535 nm, 570–700 nm can be assigned to the electron transition of $S_1 \rightarrow S_n$ and IMCT* state ($PTCDA^+ \bullet PTCDA^-$) [40]. The peak of polarized exciton ($Pe^+ \bullet Pe^-$)* can be found at 700–800 nm, in which the peak at ~740 nm belongs to the absorption of Pe^+ cations.[63,64] These above negative GB and SE peaks are also consistent with the corresponding UV-Vis absorption and PL spectra (see Fig. 3).

As compared with the fsTA spectra of CoPc and PTCDA themselves, two obvious phenomena can be found in the fsTA spectra of CoPc/PTCDA composite. 1) The positive ESA peaks of Pc ring at ~479 nm disappear, followed by the decrease of negative GB peak of PTCDA at ~480 nm. This is the typical process of energy transfer from Pc moiety in CoPc to Pe ring in PTCDA, that is, CoPc*+PTCDA →CoPc+PTCDA*. The result directly confirms the energy transfer from CoPc to PTCDA through the resonance model between two conjugated rings, as revealed through their UV-Vis and PL spectra in Fig. 3. As a result, the positive ESA peak of Pe ring at ~535 nm is stronger in CoPc/PTCDA composite than individual PTCDA. 2) The negative GB peak of CoPc LMCT state at ~609 nm becomes weak, accompanied by the disappearance of positive ESA peaks of PTCDA aggregate (PTCDA polarized exciton, $PTCDA^+ + PTCDA^-$) at 570–700 nm. Meanwhile, the positive ESA peak of CoPc LMCT* at ~645 nm and negative GB peak of PTCDA aggregate obviously enhances in CoPc/PTCDA heterojunction, as compared with those of single CoPc and PTCDA. The phenomenon verifies the excited electron transfer from $PTCDA^-$ anion in polar exciton ($PTCDA^+ \bullet PTCDA^-$) to Co atom in CoPc through the oxygen group to Co atom in CoPc (Pe→O→Co) in the CoPc/PTCDA composite. It also means that the excited electrons from Pc ligand can transfer to Co through PTCDA, and a new path of LMCT forms in CoPc, that is, Pc*→PTCDA*→Co. This is the real formation mechanism of Z-Scheme CoPc/PTCDA heterojunction. Subsequently, the peak of residual $PTCDA^+$ cationic and LMCT* excited state at 700–800 nm becomes stronger in CoPc/PTCDA heterojunction than single PTCDA and CoPc. Here, the $PTCDA^+/Pe^+$ cation is the real active site for POE [65]. The electron transfer process of Pe→O→Co can be also detected through the fsTA kinetics, as shown in Fig. 7d-f. Three obvious changes can be found after fitting the corresponding GB and ESA peaks. 1) The τ_{CR} of Pe* excited state at 535 nm decrease from 8.10 ps to 4.25 ps, and the τ_{CS} of Pe at 480 nm increase from 1.06 ps to 18.40 ps due to the de-excitation emission of π* electron ($S_n \rightarrow S_0$). 2) The τ_{CS} of CoPc LMCT state at 609 nm reduces from 1.39 ps to 0.42 ps, and the τ_{CR} of LMCT* state at 645 nm prolongs from 2.95 ps to 44.83 ps. 3) The τ_{CR} of $PTCDA^+/Pe^+$ state at ~740 nm increase from 2.13 ps to 20.13 ps, which will significantly promote the POE process. In general, the FRET from CoPc to Pe ring at UV region occurs, and the excited π electron in PTCDA conjugated ring transfer from oxygen group in PTCDA to Co atom through Co-O bond upon the light irradiation of 390 nm. The whole photoinduced energy transfer and POE mechanism in CoPc/PTCDA composite can be illustrated in Scheme 1. The above two processes of energy transfer between CoPc and PTCDA should be the radical reasons why the POE activity of CoPc/PTCDA composites is higher than that of single PTCDA, especially under the full-spectrum irradiation.

Combining the experimental results from SEM, TEM, XRD, FT-IR, and XPS etc., it can be found that there should be the coordinated interaction and hydrogen bond between oxygen groups of PTCDA and Co(II) and hydrogen atoms of CoPc besides intermolecular π-π interaction. As a result, the aggregation of CoPc (or PTCDA) molecules can be suppressed to some degree, on the contrary, they can be easily coated on 1D PTCDA (or CoPc) nanostructure to form the CoPc/PTCDA heterojunction with the decrease of CoPc (or PTCDA). Meanwhile, the planarity and rigidity of CoPc and PTCDA should enhance, and the vibration of corresponding functional groups decreases. More importantly, under the UV-Vis light irradiation, the FRET process from Pc ring to PTCDA can easily occur at the near distance, and the photoinduced electron of PTCDA can quickly transfer from oxygen group in PTCDA to Co and/or hydrogen atoms in CoPc. In this kind of Z-Scheme p/n type CoPc/PTCDA heterojunctions, the two photoinduced processes can greatly enhance the generation, separation and transportation of photoinduced carriers. Subsequently, the excited electrons and holes with the strongest redox ability can stay in the LUMO energy level of CoPc and HOMO energy level of PTCDA, respectively. Finally, water can be easily oxidized to oxygen on PTCDA, while $AgNO_3$ as electron acceptor can be reduced to Ag on CoPc during the photocatalysis.

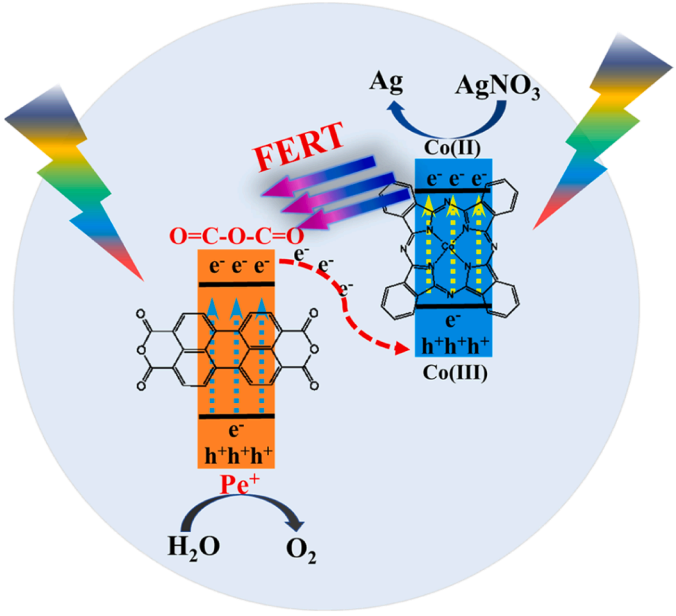

Scheme 1. The structure and POE mechanism of CoPc/PTCDA heterojunction with $AgNO_3$ as electron acceptor.

4. Conclusion

In conclusion, the organic donor/acceptor composites of p-type CoPc and n-type PTCDA molecule semiconductors with different mass ratio have been firstly prepared for photocatalytic water oxidation as catalyst. The systematical characterizations confirmed the formation of p/n type CoPc/PTCDA heterojunction due to the interaction between Co in CoPc and oxygen groups in PTCDA besides π-π interaction. A series of experiments manifested that the FRET can occur from CoPc to PTCDA in the CoPc/PTCDA composites, and 1:4 CoPc/PTCDA sample should have the best excellent POE activity under UV-Vis light irradiation. The optimal POE rate of 12.30 $mmol.g^{-1}.h^{-1}$ can be achieved ($\lambda > 420$ nm), as compared 1.58 $mmol \cdot g^{-1} \cdot h^{-1}$ of PTCDA. The AQY of 4.00 % is at 475 nm. Under the full spectrum ($\lambda > 320$ nm), the POE rate can be up to 17.65 $mmol.g^{-1}. h^{-1}$ due to the FRET from CoPc and PTCDA and their absorption for ultraviolet light. The fsTA spectra clearly revealed the existence of dual-channel energy transfer of FRET and ET between PTCDA and CoPc under the UV-Vis light, confirming the formation of Z-scheme p/n CoPc/PTCDA heterojunction. As a result, the longer exciton lifetime of MLCT (44.83 vs. 2.95 ps) and Pe^+ (20.13 vs. 2.13 ps) can be obtained in CoPc/PTCDA composites than individual CoPc and PTCDA. This work exhibited an efficient way to construct Z-scheme p/n heterojunction of organic donor/acceptor composites for photocatalytic

water splitting.

CRediT authorship contribution statement

Junqiang Li: Resources, Writing – original draft, Writing – review & editing. **Shoufeng Wang:** Validation, Formal analysis, Data curation. **Renfu Li:** Methodology, Data curation. **Bo Zhang:** Validation, Data curation. **Xiao Xu:** Software, Data curation. **Zhuoyue Wang:** Methodology, Formal analysis. **Longtian Kang:** Conceptualization, Methodology, Writing – review & editing, Supervision, Project administration.

Declaration of Competing Interest

The authors declare that they have no known competing financial interests or personal relationships that could have appeared to influence the work reported in this paper.

Data availability

No data was used for the research described in the article.

Acknowledgements

The Fujian Science & Technology Innovation Laboratory for Optoelectronic Information of China (2021ZR124) provided funding for this research.

Appendix A. Supporting information

Supplementary data associated with this article can be found in the online version at doi:10.1016/j.apcatb.2023.123381.

References

[1] L. Lin, T. Hisatomi, S. Chen, T. Takata, K. Domen, Visible-light-driven photocatalytic water splitting: recent progress and challenges, Trends Chem. 2 (2020) 813–824, https://doi.org/10.1016/j.trechm.2020.06.006.
[2] C. Zhao, Z. Chen, R. Shi, X. Yang, T. Zhang, Recent advances in conjugated polymers for visible-light-driven water splitting, Adv. Mater. 32 (2020), e1907296, https://doi.org/10.1002/adma.201907296.
[3] Y. Chen, C. Yan, J. Dong, W. Zhou, F. Rosei, Y. Feng, L.N. Wang, Structure/property control in photocatalytic organic semiconductor nanocrystals, Adv. Funct. Mater. 31 (2021), 2104099, https://doi.org/10.1002/adfm.202104099.
[4] J.J. Wei, X. Chen, X.T. Ren, S.F. Tian, F. Bai, Facile construction of intramolecular g-CN-PTCDA donor-acceptor system for efficient CO_2 photoreduction, Catalysts 13 (2023) 600, https://doi.org/10.3390/catal13030600.
[5] Y. Fang, Y. Hou, X. Fu, X. Wang, Semiconducting polymers for oxygen evolution reaction under light illumination, Chem. Rev. 122 (2022) 4204–4256, https://doi.org/10.1021/acs.chemrev.1c00686.
[6] Q. Guo, Z. Ma, C. Zhou, Z. Ren, X. Yang, Single molecule photocatalysis on TiO_2 surfaces, Chem. Rev. 119 (2019) 11020–11041, https://doi.org/10.1021/acs.chemrev.9b00226.
[7] J. Yang, S. He, H. Liu, E. Jaatinen, E. Waclawik, J. Quan, S. Sarina, C. He, S. Huang, H. Zhu, M. Wu, Enhancing visible-light photocatalytic performance of Au/TiO_2 catalysts through light reflection-promoted optical absorption with oriented anatase mesocrystals, J. Mater. Chem. A 11 (2023) 4751–4757, https://doi.org/10.1039/d2ta09982a.
[8] D. Dai, X. Liang, B. Zhang, Y. Wang, Q. Wu, X. Bao, Z. Wang, Z. Zheng, H. Cheng, Y. Dai, B. Huang, P. Wang, Strain adjustment realizes the photocatalytic overall water splitting on tetragonal zircon $BiVO_4$, Adv. Sci. 9 (2022) 2105299, https://doi.org/10.1002/advs.202105299.
[9] H.J. Kong, K.-H. Kim, S. Kim, H. Lee, J.K. Kang, Unveiling the role of tetragonal $BiVO_4$ as a mediator for dual phase $BiVO_4$/g-C_3N_4 composite photocatalysts enabling highly efficient water oxidation via Z-scheme charge transfer, J. Mater. Chem. A 7 (2019) 26279–26284, https://doi.org/10.1039/c9ta10704e.
[10] N. Zhang, C. Chen, Z. Mei, X. Liu, X. Qu, Y. Li, S. Li, W. Qi, Y. Zhang, J. Ye, V.A. L. Roy, R. Ma, Monoclinic tungsten oxide with {100} facet orientation and tuned electronic band structure for enhanced photocatalytic oxidations, ACS Appl. Mater. Interfaces 8 (2016) 10367–10374, https://doi.org/10.1021/acsami.6b02275.
[11] J. Kosco, F. Moruzzi, B. Willner, I. McCulloch, Photocatalysts based on organic semiconductors with tunable energy levels for solar fuel applications, Adv. Energy Mater. 10 (2020), 2001935, https://doi.org/10.1002/aenm.202001935.
[12] Q. Chen, Y. Zhang, E. You, Q. Jiang, X. Chen, Y. Wang, Z. Song, K. Chang, Z. Xie, Q. Kuang, Accelerated water oxidation kinetics triggered by supramolecular porphyrin nanosheet for robust visible-light-driven CO_2 reduction, Small 18 (2022), 2204924, https://doi.org/10.1002/smll.202204924.
[13] E. Nikoloudakis, I.L. Duarte, G. Charalambidis, K. Ladomenou, M. Ince, A. G. Coutsolelos, Porphyrins and phthalocyanines as biomimetic tools for photocatalytic H_2 production and CO_2 reduction, Chem. Soc. Rev. 51 (2022) 6965–7045, https://doi.org/10.1039/d2cs00183g.
[14] J. Yang, J. Jing, W. Li, Y. Zhu, Electron donor-acceptor interface of TPPS/PDI boosting charge transfer for efficient photocatalytic hydrogen evolution, Adv. Sci. 9 (2022), e2201134, https://doi.org/10.1002/advs.202201134.
[15] Y. Cao, H. Gou, P. Zhu, Z. Jin, Ingenious design of CoAl-LDH p-n heterojunction based on CuI as holes receptor for photocatalytic hydrogen evolution, Chin. J. Struct. Chem. 41 (2022) 2206079–2206085, http://manu30.magtech.com.cn/jghx/EN/10.14102/j.cnki.0254-5861.2022-0042.
[16] X. Li, C. Garlisi, Q.S. Guan, S. Anwer, K.A. Ali, G. Palmisano, L.X. Zheng, A review of material aspects in developing direct Z-scheme photocatalysts, Mater. Today 47 (2021) 75–107, https://doi.org/10.1016/j.mattod.2021.02.017.
[17] K. Chen, J. Xiao, J.J.M. Vequizo, T. Hisatomi, Y. Ma, M. Nakabayashi, T. Takata, A. Yamakata, N. Shibata, K. Domen, Overall water splitting by a $SrTaO_2N$-based photocatalyst decorated with an Ir-promoted Ru-based cocatalyst, J. Am. Chem. Soc. 145 (2023) 3839–3843, https://doi.org/10.1021/jacs.2c11025.
[18] Z. Lin, Y.Q. Wang, Z.M. Peng, Y.C. Huang, F.Q. Meng, E.L. Chen, C.L. Dong, Q. H. Zhang, R.Z. Wang, D.M. Zhao, J. Chen, L. Gu, S.H. Shen, Single-metal atoms and ultra-small clusters manipulating charge carrier migration in polymeric perylene diimide for efficient photocatalytic oxygen production, Adv. Energy Mater. 12 (2022), 2200716, https://doi.org/10.1002/aenm.202200716.
[19] Y. Sheng, W. Li, L. Xu, Y. Zhu, High photocatalytic oxygen evolution via strong built-in electric field induced by high crystallinity of perylene imide supramolecule, Adv. Mater. 34 (2022), e2102354, https://doi.org/10.1002/adma.202102354.
[20] A. Sabbah, I. Shown, M. Qorbani, F.Y. Fu, T.Y. Lin, H.L. Wu, P.W. Chung, C.I. Wu, S.R.M. Santiago, J.L. Shen, K.H. Chen, L.C. Chen, Boosting photocatalytic CO_2 reduction in a ZnS/$ZnIn_2S_4$ heterostructure through strain-induced direct Z-scheme and a mechanistic study of molecular CO_2 interaction thereon, Nano Energy 93 (2022), 106809, https://doi.org/10.1016/j.nanoen.2021.106809.
[21] X. He, T. Kai, P. Ding, Heterojunction photocatalysts for degradation of the tetracycline antibiotic: a review, Environ. Chem. Lett. 19 (2021) 4563–4601, https://doi.org/10.1007/s10311-021-01295-8.
[22] J. Abdul Nasir, A. Munir, N. Ahmad, T.U. Haq, Z. Khan, Z. Rehman, Photocatalytic Z-scheme overall water splitting: recent advances in theory and experiments, Adv. Mater. 33 (2021), e2105195, https://doi.org/10.1002/adma.202105195.
[23] G.F. Liao, C.X. Li, S.Y. Liu, B.Z. Fang, H.M. Yang, Z-scheme systems: from fundamental principles to characterization, synthesis, and photocatalytic fuel-conversion applications, Phys. Rep. 983 (2022) 1–41, https://doi.org/10.1016/j.physrep.2022.07.003.
[24] X.D. Zhang, J. Yan, L.Y.S. Lee, Highly promoted hydrogen production enabled by interfacial P-N chemical bonds in copper phosphosulfide Z-scheme composite, Appl. Catal. B Environ. 283 (2021), 119624, https://doi.org/10.1016/j.apcatb.2020.119624.
[25] G.B. Miao, M. Zhou, Y.Y. Zhang, Z.F. Yang, Y.L. Liu, Nanoarchitectonic composites with direct z-scheme heterojunction of $CsPbBr_3$ quantum dot/$CuCo_2O_4$ nanosheet for efficient photocatalytic CO_2 reduction, J. Alloy. Compd. 925 (2022), 166733, https://doi.org/10.1016/j.jallcom.2022.166733.
[26] H. Zhang, X.F. Bai, Photocatalytic production of hydrogen peroxide over Z-scheme Mn_3O_4/Co_9S_8 with p-n heterostructure, Appl. Catal. B Environ. 298 (2021), 120516, https://doi.org/10.1016/j.apcatb.2021.120516.
[27] Z. Zhong, J.J. Liu, X. Xu, A.H. Cao, Z.J. Tao, W.F. You, L.T. Kang, Synthesis of Z-scheme cobalt porphyrin/nitrogen-doped graphene quantum dot heterojunctions for efficient molecule-based photocatalytic oxygen evolution, J. Mater. Chem. A 9 (2021) 2404–2413, https://doi.org/10.1039/d0ta10196f.
[28] Y.J. Yuan, Z.K. Shen, P. Wang, Z.J. Li, L. Pei, J.S. Zhong, Z.G. Ji, Z.T. Yu, Z.G. Zou, Metal-free broad-spectrum PTCDA/g-C_3N_4 Z-scheme photocatalysts for enhanced photocatalytic water oxidation, Appl. Catal. B Environ. 260 (2020), 118179, https://doi.org/10.1016/j.apcatb.2019.118179.
[29] S. Chang, J. Yu, R. Wang, Q. Fu, X. Xu, $LaTaON_2$ Mesoporous single crystals for efficient photocatalytic water oxidation and Z-scheme overall eater splitting, ACS Nano 15 (2021) 18153–18162, https://doi.org/10.1021/acsnano.1c06871.
[30] X. Yang, Z. Chen, J. Xu, H. Tang, K. Chen, Y. Jiang, Tuning the morphology of g-C_3N_4 for improvement of Z-scheme photocatalytic water oxidation, ACS Appl. Mater. Interfaces 7 (2015) 15285–15293, https://doi.org/10.1021/acsami.5b02649.
[31] A.J.P. Teunissen, C.P. Medina, A. Meijerink, W.J.M. Mulder, Investigating supramolecular systems using forster resonance energy transfer, Chem. Soc. Rev. 47 (2018) 7027–7044, https://doi.org/10.1039/c8cs00278a.
[32] H.H. Li, L.L. Jie, J.N. Pan, L.T. Kang, J.N. Yao, Direct photocatalytic hydrogen evolution from water splitting using nanostructures of hydrate organic small molecule as photocatalysts, J. Mater. Chem. A 4 (2016) 6577–6584, https://doi.org/10.1039/c6ta01582d.
[33] K. Zheng, G.B. Bodedla, Y. Hou, J. Zhang, R. Liang, J. Zhao, D. Lee Phillips, X. Zhu, Enhanced cocatalyst-free photocatalytic H_2 evolution by the synergistic AIE and FRET for an Ir-complex conjugated porphyrin, J. Mater. Chem. A 10 (2022) 4440–4445, https://doi.org/10.1039/d1ta10294j.
[34] Y. Li, X. Zhang, D. Liu, Recent developments of perylene diimide (PDI) supramolecular photocatalysts: a review, J. Photochem. Photobiol. C 48 (2021), 100436, https://doi.org/10.1016/j.jphotochemrev.2021.100436.
[35] D. Powell, L.W. Brooks, Concepts and principles of self-n-doping in perylene diimide chromophores for applications in biochemistry, energy harvesting, energy storage, and catalysis, Mater. Horiz. 9 (2022) 2026–2052, https://doi.org/10.1039/d2mh00279e.

[36] Y.R. Xu, X.D. Zhu, H. Yan, P.P. Wang, M.S. Song, C.C. Ma, Z.R. Chen, J.Y. Chu, X. L. Liu, Z.Y. Lu, Hydrochloric acid-mediated synthesis of $ZnFe_2O_4$ small particle decorated one-dimensional perylene diimide S-scheme heterojunction with excellent photocatalytic ability, Chin. J. Catal. 43 (2022) 1111–1122, https://doi.org/10.1016/S1872-2067(21)63930-X.
[37] E.E. Greciano, J. Calbo, E. Orti, L. Sanchez, N-annulated perylene bisimides to bias the differentiation of metastable supramolecular assemblies into J- and H-Aggregates, Angew. Chem. Int. Ed. 59 (2020) 17517–17524, https://doi.org/10.1002/anie.202005837.
[38] H. Ding, Z. Wang, K. Kong, S. Feng, L. Xu, H. Ye, W. Wu, X. Gong, J. Hua, Efficient and stable photocatalytic H_2 evolution by self-assembly of zirconium(iv) coordination with perylene diimide supramolecules under visible light irradiation, J. Mater. Chem. A 9 (2021) 7675–7683, https://doi.org/10.1039/d1ta00464f.
[39] J.X. Li, Z.J. Li, C. Ye, X.B. Li, F. Zhan, X.B. Fan, J. Li, B. Chen, Y. Tao, C.H. Tung, L. Z. Wu, Visible light-induced photochemical oxygen evolution from water by 3,4,9,10-perylenetetracarboxylic dianhydride nanorods as an n-type organic semiconductor, Cryst. Res. Technol. 6 (2016) 672–676, https://doi.org/10.1039/c5cy01570g.
[40] A. Cao, R. Li, X. Xu, W. Huang, Y. He, J. Li, M. Sun, X. Chen, L. Kang, Cobalt-intercalated one-dimensional nanocrystals of urea perylene imide polymer for enhanced visible-light photocatalytic water oxidation, Appl. Catal. B Environ. 309 (2022), 121293, https://doi.org/10.1016/j.apcatb.2022.121293.
[41] G. Cao, D. Qin, J. Cao, M. Guan, Y. Zeng, J. Li, Improved performance in organic light emitting diodes with a mixed electron donor-acceptor film involved in hole injection, J. Appl. Phys. 101 (2007), 124507, https://doi.org/10.1063/1.2747594.
[42] M. Hirade, H. Nakanotani, M. Yahiro, C. Adachi, Formation of organic crystalline nanopillar arrays and their application to organic photovoltaic cells, ACS Appl. Mater. Interfaces 3 (2011) 80–83, https://doi.org/10.1021/am100915s.
[43] R. Schlaf, B.A. Parkinson, P.A. Lee, K.W. Nebesny, N.R. Armstrong, HOMO/LUMO alignment at PTCDA/ZnPc and PTCDA/ClInPc heterointerfaces determined by combined UPS and XPS measurements, J. Phys. Chem. B 103 (1999) 2984–2992, https://doi.org/10.1021/jp982834y.
[44] Y. Huang, Z. Wang, Z. Chen, Q. Zhang, Organic cocrystals: beyond electrical conductivities and field-effect transistors (FETs), Angew. Chem. Int. Ed. 58 (2019) 9696–9711, https://doi.org/10.1002/anie.201900501.
[45] J. Li, W. Huang, Z. Wang, X. Xu, M. Sun, L. Kang, Controllable dispersion of cobalt phthalocyanine molecules on graphene oxide for enhanced photocatalytic CO_2 reduction, Mol. Catal. 546 (2023), 113253, https://doi.org/10.1016/j.mcat.2023.113253.
[46] N.S. Nikolaeva, D.D. Klyamer, S.M. Zharkov, A.R. Tsygankova, A.S. Sukhikh, N. B. Morozova, T.V. Basova, Heterostructures based on Pd–Au nanoparticles and cobalt phthalocyanine for hydrogen chemiresistive sensors, Int. J. Hydrog. Energy 46 (2021) 19682–19692, https://doi.org/10.1016/j.ijhydene.2021.03.082.
[47] X. Ji, T. Zou, H. Gong, Q. Wu, Z. Qiao, W. Wu, H. Wang, Cobalt phthalocyanine nanowires: growth, crystal structure, and optical properties, Cryst. Res. Technol. 51 (2016) 154–159, https://doi.org/10.1002/crat.201500244.
[48] X. Wang, C. Bommier, Z. Jian, Z. Li, R.S. Chandrabose, I.A.R. Perez, P.A. Greaney, X. Ji, Hydronium-ion batteries with perylenetetracarboxylic dianhydride crystals as an electrode, Angew. Chem. Int. Ed. 56 (2017) 2909–2913, https://doi.org/10.1002/anie.201700148.
[49] W.F. Huang, J.Q. Li, X. Xu, A.H. Cao, Y. He, M. Sun, L.T. Kang, Controllable dispersion of cobalt phthalocyanine molecules on graphene oxide for enhanced electrocatalytic reduction of CO_2 to CO, New J. Chem. 46 (2022) 7153–7160, https://doi.org/10.1039/d1nj06182h.
[50] Y. Wang, H. Wu, W. Zhu, X. Zhang, Z. Liu, Y. Wu, C. Feng, Y. Dang, H. Dong, H. Fu, W. Hu, Cocrystal engineering: toward solution-processed near-infrared 2D organic cocrystals for broadband photodetection, Angew. Chem. Int. Ed. 60 (2021) 6344–6350, https://doi.org/10.1002/anie.202015326.
[51] K. Akers, R. Aroca, A.M. Hor, R.O. Loutfy, Molecular-organization in perylenetetracarboxylic dianhydride films, J. Phys. Chem. 91 (1987) 2954–2959, https://doi.org/10.1021/j100295a061.
[52] F. Mo, J. Guo, M. Chen, H. Meng, Y. Fu, Gold nanoparticles photosensitization towards 3,4,9,10-perylenetetracarboxylic dianhydride integrated with a dual-particle three-dimensional DNA roller: a general "ON-OFF-ON" photoelectric plasmon-rnhanced biosensor, Anal. Chem. 93 (2021) 10947–10954, https://doi.org/10.1021/acs.analchem.1c01816.
[53] J. Zhou, Y. Wang, Z. Cui, Y. Hu, X. Hao, Y. Wang, Z. Zou, Ultrathin conjugated polymer nanosheets as highly efficient photocatalyst for visible light driven oxygen activation, Appl. Catal. B Environ. 277 (2020), 119228, https://doi.org/10.1016/j.apcatb.2020.119228.
[54] W. Li, X. Li, X. Fu, Z. Lou, Y. Zhu, Y. Zhang, Photo-induced conversion of type-II CoPc/BiOBr-NSs to S-scheme heterostructure for boosting CO_2 photoreduction, Chem. Eng. J. 451 (2023), 138932, https://doi.org/10.1016/j.cej.2022.138932.
[55] R. Sun, Y.L. Wang, Z.Q. Zhang, Y. Qu, Z.J. Li, B. Li, H.J. Wu, X.Y. Hua, S.Y. Zhang, F.J. Zhang, L.Q. Jing, Ultrathin phosphate-modulated zinc phthalocyanine/perylenete diimide supermolecule Z-scheme heterojunctions as efficiently wide visible-light photocatalysts for CO_2 conversion, Chem. Eng. J. 426 (2021), 131266, https://doi.org/10.1016/j.cej.2021.131266.
[56] T. Enokida, R. Hirohashi, Cobalt phthalocyanine crystal dynthesized at low-temperature, Chem. Mater. 3 (1991) 918–921, https://doi.org/10.1021/cm00017a030.
[57] X. Tan, C. Yu, X. Song, C. Zhao, S. Cui, H. Xu, J. Chang, W. Guo, Z. Wang, Y. Xie, J. Qiu, Toward an understanding of the enhanced CO_2 electroreduction in NaCl electrolyte over CoPc molecule-implanted graphitic carbon nitride catalyst, Adv. Energy Mater. 11 (2021), 2100075, https://doi.org/10.1002/aenm.202100075.
[58] Y. Kim, D. Kim, J. Lee, L.Y.S. Lee, D.K.P. Ng, Tuning the electrochemical properties of polymeric cobalt phthalocyanines for efficient water splitting, Adv. Funct. Mater. 31 (2021), 2103290, https://doi.org/10.1002/adfm.202103290.
[59] M. Wang, K. Ishii, Photochemical properties of phthalocyanines with transition metal ions, in: Coord. Chem. Rev, 468, 2022, 214626, https://doi.org/10.1016/j.ccr.2022.214626.
[60] L. Zhang, X. Hao, J. Li, Y. Wang, Z. Jin, Unique synergistic effects of ZIF-9(Co)-derived cobalt phosphide and $CeVO_4$ heterojunction for efficient hydrogen evolution, Chin. J. Catal. 41 (2020) 82–94, https://doi.org/10.1016/S1872-2067(19)63454-6.
[61] J. Zheng, Z. Lei, Incorporation of CoO nanoparticles in 3D marigold flower like hierarchical architecture $MnCo_2O_4$ for highly boosting solar light photo oxidation and reduction ability, Appl. Catal. B Environ. 237 (2018) 1–8, https://doi.org/10.1016/j.apcatb.2018.05.060.
[62] D. Xu, B. Cheng, W. Wang, C. Jiang, J. Yu, Ag_2CrO_4/g-C_3N_4/graphene oxide ternary nanocomposite Z-scheme photocatalyst with enhanced CO_2 reduction activity, Appl. Catal. B Environ. 231 (2018) 368–380, https://doi.org/10.1016/j.apcatb.2018.03.036.
[63] T. Kim, C. Lin, J.D. Schultz, R.M. Young, M.R. Wasielewski, π-Stacking-dependent vibronic Couplings drive excited-state dynamics in perylenediimide assemblies, J. Am. Chem. Soc. 144 (2022) 11386–11396, https://doi.org/10.1021/jacs.2c03993.
[64] C. Qin, Z. Zhang, Q. Xu, J. Song, Z. Jiao, S. Ma, R. Qin, Y. Jiang, Direct observation of ultrafast delaxation dynamics of a mixed excimer state in perylene monoimide dimer by femtosecond transient absorption, J. Phys. Chem. Lett. 14 (2023) 2455–2462, https://doi.org/10.1021/acs.jpclett.3c00106.
[65] J. Zhang, Z.J. Wang, J.Y. Shi, W.B. Zhu, L. Yang, Y. Wang, Z.G. Zou, Bay-monosubstitution with electron-donating group as an efficiently strategy to functionalize perylene imide polymer for enhancing photocatalytic oxygen evolution activity, Adv. Funct. Mater. 32 (2022), 2205895, https://doi.org/10.1002/adfm.202205895.